Scattering of radio frequency waves by blob-filaments

J. R. Myra and D. A. D'Ippolito

July 2010

submitted to *Phys. Plasmas*

DOE/ER/54392-58 & DOE/ER/54823-10 LRC-10-134

LODESTAR RESEARCH CORPORATION
2400 Central Avenue
Boulder, Colorado 80301

Scattering of radio frequency waves by blob-filaments

J. R. Myra and D. A. D'Ippolito

Lodestar Research Corp., 2400 Central Ave. P-5, Boulder, Colorado 80301

Abstract

Radio frequency waves used for heating and current drive in magnetic confinement experiments must traverse the scrape-off-layer (SOL) and edge plasma before reaching the core. The edge and SOL plasmas are strongly turbulent and intermittent in both space and time. As a first approximation, the SOL can be treated as a tenuous background plasma upon which denser filamentary field-aligned blobs of plasma are superimposed. The blobs are approximately stationary on the rf time-scale. The scattering of fast and slow plane-waves in the ion-cyclotron to lower-hybrid frequency range from a cylindrical blob is treated here in the cold plasma model. Scattering widths are derived for incident fast and slow waves, and the scattered power fraction is estimated. Processes such as scattering-induced mode conversion, scattering resonances, and shadowing are investigated.

PACS: 52.25.Os, 52.35.Ra, 52.50.Qt, 52.55.Fa

I. Introduction

Ion cyclotron range of frequency (ICRF) waves and lower-hybrid (LH) waves have been successfully employed for heating and current drive in magnetic confinement experiments for many decades. These radio-frequency waves must traverse the scrape-off-layer (SOL) and edge plasmas before they can perform their intended functions in the core plasma.

Most present day numerical rf codes treat the propagation of the waves through the edge and SOL plasmas in relatively simple linear models in which the background plasma is steady state, laminar, and one dimensional (varying only in the flux coordinate). In reality, this tenuous plasma is strongly turbulent and intermittent in both space and time.[1] A typical auto-correlation time scale for turbulent structures is on the order of 10 μs, and the correlation lengths are on the order of 1 cm in the direction perpendicular to the background magnetic field B_0, and much longer, perhaps 10 m or more parallel to B_0. Furthermore, fluctuation amplitudes in the far SOL are of order unity and are dominated by intermittent convection of blob-filaments and edge-localized modes (ELMs).[2,3] These filamentary structures, which we will refer to simply as "blobs" in the following, consist of flux tubes containing denser plasma than the background. The excess density can exceed that of the background by factors much larger than unity. Relative to the short rf period for ICRF and LH waves (<< 1 μs), the turbulent structures are frozen in time, but present a spatially intermittent SOL to the waves.

It is to be expected that propagating waves would scatter off of the plasma fluctuations. Indeed there is both experimental evidence for such scattering,[4,5] and previous theoretical treatments of the problem.[6-8] The standard theoretical paradigm has been to model the fluctuations as a randomized spectrum of plane wave perturbations superimposed on a background plasma. Then the trajectory of the waves in configuration and k-space, upon encountering many scattering events, can be treated in a Fokker-Planck approximation. This approach has provided many useful insights.

In the present paper we take a somewhat different and complementary approach, motivated by recent advances in SOL turbulence and blob dynamics.[2,3] Specifically we consider the interaction of an rf wave with a single blob-filament. This limit is particularly interesting for the far SOL, where the blob events are large but rare and therefore relatively isolated from each other.

To model this situations, in this paper, we compute the scattering of a plane wave from a cylinder of higher (or perhaps lower) constant density plasma, i.e. a blob (or "hole"). The geometry is shown in Fig. 1. The primary quantity of interest is the scattered power and its spatial distribution, i.e. the total and differential scattering cross-section or width. (Because of assumed symmetry along the axis of the cylinder, the scattering width is just the scattering cross-section per unit length). The calculation is a generalization of the classical problem of scalar wave scattering from a metal cylinder that is treated in standard textbooks.[9] Here, however, we must address the complications introduced by vector wave-fields, the anisotropic magnetized plasma dielectric tensor, and electromagnetic matching conditions across the interface between the blob and background plasma. Nevertheless, as we shall see, the problem is still amenable to a treatment in terms of Bessel and Hankel functions.

Two cases are considered: (i) an incident fast wave (FW) (motivated by ICRF applications), and (ii) an incident slow wave (SW) (motivated by LH applications). The formalism is discussed in Sec. II and in the Appendices, while the applications to the FW and SW are discussed in Secs. III and IV respectively. Conclusions are given in Sec. V.

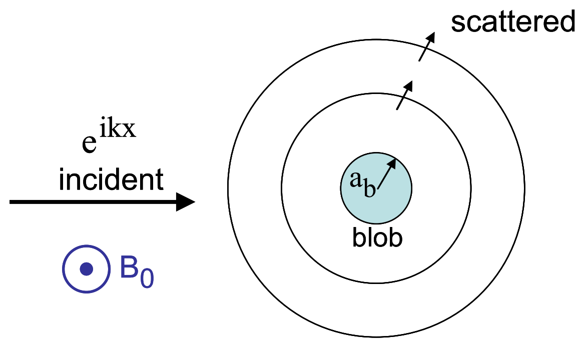

Fig. 1 (color online) Geometry for rf blob scattering. The plasma parameters are taken as constants in the background and in the blob.

II. Scattering formalism

In order to calculate rf scattering from blobs in our model, it is necessary to solve the FW and SW equations in cylindrical geometry, (r, θ, z) with the background magnetic field $\mathbf{B}_0 = B_0\mathbf{e}_z$ along the axis of the cylinder. For a homogeneous plasma, the FW and SW are normally decoupled when $\varepsilon_{||} >> \varepsilon_\perp$ where the cold-fluid dielectric tensor is represented as

$$\varepsilon = \varepsilon_\perp \mathrm{I} + \mathbf{bb}(\varepsilon_{||} - \varepsilon_\perp) + i\varepsilon_\times \mathbf{b} \times \mathrm{I} \tag{1}$$

where $\mathbf{b} = \mathbf{B}_0/B_0 = \mathbf{e}_z$. For the present range of applications to ICRF and LH waves in the low density SOL plasma, the following approximations are adequate: $\varepsilon_\perp = 1 + \omega_{pi}^2/(\Omega_i^2 - \omega^2)$, $\varepsilon_{||} = 1 - \omega_{pe}^2/\omega^2$, $\varepsilon_\times = \omega_{pi}^2\omega/\Omega_i(\omega^2 - \Omega_i^2)$ where ω_{pi}, ω_{pe} and Ω_i are the ion plasma, electron plasma and ion cyclotron frequencies respectively. The reduced wave equations for the FW and SW in cylindrical geometry are derived in Appendix A.

For the FW, which obeys the ordering $\varepsilon_{||} >> \varepsilon_\perp \sim n_\perp^2 \sim n_{||}^2$, the decoupling of FW and SW amounts to neglecting E_z to obtain

$$\left(\varepsilon_\perp - n_{||}^2 - \lambda_0^2\frac{m^2}{r^2}\right)E_r = i\varepsilon_\times E_\theta + \lambda_0^2\frac{im}{r^2}\frac{d}{dr}(rE_\theta) \tag{2}$$

$$\lambda_0^2 \frac{d}{dr}\left(\frac{1}{r}\frac{d}{dr}(rE_\theta)\right) + (\varepsilon_\perp - n_\parallel^2)E_\theta + i\varepsilon_\times E_r - im\lambda_0^2 \frac{d}{dr}\left(\frac{E_r}{r}\right) = 0 \tag{3}$$

where $n_\parallel = k_\parallel c/\omega$, $\lambda_0 = c/\omega$, and all wave fields are proportional to $\exp(im\theta + ik_\parallel z - i\omega t)$.

For the SW, which obeys the ordering $\varepsilon_\parallel \sim n_\perp^2 >> \varepsilon_\perp \sim n_\parallel^2$, the calculation in Appendix A shows that $\mathbf{E}_\perp = -\nabla_\perp \Phi$ where Φ and E_z obey

$$(\varepsilon_\perp - n_\parallel^2)\nabla_\perp^2 \Phi + ik_\parallel \lambda_0^2 \nabla_\perp^2 E_z = 0 \tag{4}$$

$$ik_\parallel \lambda_0^2 \nabla_\perp^2 \Phi + \lambda_0^2 \nabla_\perp^2 E_z + \varepsilon_\parallel E_z = 0 \tag{5}$$

The next step is to find general solutions to these FW and SW equations in cylindrical geometry for a given m and $k_\parallel$, i.e. we seek the radial structure of the modes. A solution of Eqs. (2) and (3) or (4) and (5) is deferred to Appendix B where it is shown that the general solution of these equations takes the form

$$\mathbf{E} = \sum_{m,j} e^{im\theta} E_m^{(j)} \mathbf{W}_m^{(j)}(r) \tag{6}$$

Here, the index j denotes the wave type (incident field, scattered field, or field internal to the blob) as well as the branch of wave (FW or SW), the $E_m^{(j)}$ are constant amplitudes to be determined, and the $\mathbf{W}_m^{(j)}(r)$ are combinations of Bessel functions. For example, for an incoming fast plane wave normalized so that E_y has unit amplitude as $x \to \infty$ it is shown that

$$E_\theta = \sum_m i^{m-1}\left(J'_m + \frac{imQJ_m}{k_\perp r}\right)e^{im\theta} \tag{7}$$

where $Q = i\varepsilon_\times/(\varepsilon_\perp - n_\parallel^2)$, all Bessel functions have argument $\xi = k_\perp r$, where r = x cos θ, and for the incoming wave $k_y = 0$ so that $k_\perp = k_x$.

Having obtained Eq. (6) as the general solution to the wave equation, it remains to satisfy boundary conditions. We choose J_m Bessel functions for the internal blob solution to give regularity at r = 0, outgoing Hankel functions for the scattered wave, and J_m Bessel functions for the plane wave expansion of the incident wave. These choices satisfy appropriate boundary conditions at zero and infinity. Finally, we apply the electromagnetic matching conditions across the blob interface at $r = a_b$, assuming no surface currents, viz. the continuity of E_θ, B_z, D_r and E_z where $\mathbf{D} = \varepsilon\cdot\mathbf{E}$, and E_θ, B_z, D_r and E_z are all rf oscillating quantities. (When these 4 quantities match, it can be shown that B_r and B_θ also match.) This matching determines the unknown coefficients $E_m^{(j)}$ in terms of the amplitude of the incident wave.

In general, the interface matching results in a 4×4 system of equations for the internal blob and scattered amplitudes of both FW and SW polarizations. That is, the scattering process in general mixes the FW and SW polarizations. When the mixing of polarizations can be neglected, the 4×4 system reduces to 2×2 blocks for the FW and SW respectively.

To be more explicit let

$$j = \begin{cases} 0 & \text{incident wave type } p \\ 1 & \text{scattered wave type } p \\ 2 & \text{scattered wave type } p' \\ 3 & \text{blob wave type } p \\ 4 & \text{blob wave type } p' \end{cases} \tag{8}$$

where the fields j = 0, 1, 2 apply for $r > a_b$ while j = 3, 4 apply for $r < a_b$. If p is the FW then the notation p′ implies the SW, and *vice versa*. The scattering of each m component can be treated separately because there is no explicit θ dependence in $\mathbf{W}_m^{(j)}$. This allows a simplification of notation: dropping the m index and moving the (j) from a superscript down to a subscript. With the incident wave E_0 regarded as known, one can solve for the scattered wave and the solution inside the blob. Then the 4 matching conditions at $r = a_b$ take the form

$$E_1 W_{1\theta} + E_2 W_{2\theta} - E_3 W_{3\theta} - E_4 W_{4\theta} = -E_0 W_{0\theta} \tag{9}$$

$$E_1 M_1 + E_2 M_2 - E_3 M_3 - E_4 M_4 = -E_0 M_0 \tag{10}$$

$$E_1 D_1 + E_2 D_2 - E_3 D_3 - E_4 D_4 = -E_0 D_0 \tag{11}$$

$$E_1 W_{1z} + E_2 W_{2z} - E_3 W_{3z} - E_4 W_{4z} = -E_0 W_{0z} \tag{12}$$

where

$$M_j = \frac{1}{r}\frac{d}{dr} rW_{j\theta} - \frac{im}{r} W_{jr} \quad (13)$$

$$D_j = \varepsilon_{\perp} W_{jr} - i\varepsilon_{\times} W_{j\theta} \quad (14)$$

and all quantities are evaluated at $r = a_b$. Here $E_j M_j$ is proportional to B_z while $E_j D_j$ is proportional to D_r. The FW and SW limits of this system are considered in the following sections.

The scattered power is obtained from the asymptotic forms of the outgoing Hankel functions (j = 1, 2) and the Poynting flux these waves carry (see Appendix C). The solution to Eqs. (9) – (12) gives the amplitudes of the various waves at the blob interface. These are related to the asymptotic forms as $r \to \infty$ by using the particular combination of Bessel and Hankel functions appropriate to the given FW or SW (see Appendix D). Then, the ratio of total scattered wave E_{sca} to incident wave E_{inc} can be expressed as

$$\left.\frac{E_{sca}}{E_{inc}}\right|_{r\to\infty} = \sum_m A_m e^{im\theta} \quad (15)$$

and from Appendix C the scattered power is

$$\frac{P_{sca}}{P_{inc}} = \frac{2\pi r}{L_y} \sum_m |A_m|^2 \quad (16)$$

It is then natural to define the scattered power per scattering center (i.e. blob) per incident power / L_y as the effective scattering width

$$\sigma = 2\pi r \sum_m |A_m|^2 \quad (17)$$

Finally, a heuristic estimate of the total scattered power is obtained by summing over all blobs in the path of the incident wave (neglecting multiple scattering events, and correlations, i.e. strictly valid for a sparse blob population). Let

$$\frac{P_{stot}}{P_{inc}} = \sigma \frac{N_b}{L_y} \quad (18)$$

where N_b is the number of blobs in a cross-sectional area of SOL equal to $L_x L_y$ and L_x is the length of the blob-populated SOL path of the incident rf wave. Define the packing fraction of blobs in the SOL as

$$f_p = \frac{\pi a^2 N_b}{L_x L_y} \tag{19}$$

Then the fraction of incident power scattered by all blobs in the path of length L_x is

$$F_P \equiv \frac{P_{stot}}{P_{inc}} = \frac{\sigma f_p L_x}{\pi a^2} \tag{20}$$

III. Scattering of an incident fast wave

FW limit of the formalism

Although the possibility of coupling of an incident FW to a SW by blob scattering is of interest, we begin by ignoring the SW. Later we calculate the SW fields perturbatively, noting the conditions where the perturbation theory breaks down. Neglecting the SW results in the reduced FW matching problem at $r = a_b$

$$E_1 W_{1\theta} - E_3 W_{3\theta} = -E_0 W_{0\theta} \tag{21}$$

$$E_1 M_1 - E_3 M_3 = -E_0 M_0 \tag{22}$$

and the solution

$$\frac{E_1}{E_0} = \frac{W_{3\theta} M_0 - W_{0\theta} M_3}{W_{1\theta} M_3 - W_{3\theta} M_1} \tag{23}$$

$$\frac{E_3}{E_0} = \frac{W_{1\theta} M_0 - W_{0\theta} M_1}{W_{1\theta} M_3 - W_{3\theta} M_1} \tag{24}$$

Here the Bessel-function combinations W_j and M_j have the arguments $\xi = k_\perp a_b$ for the external functions (j = 0, 1) and $\xi_b = k_{\perp b} a_b$ for the internal functions (j = 3) where $k_\perp$ and $k_{\perp b}$ are evaluated from the dispersion relation using external and internal-blob parameters respectively. Explicit forms for W_j and M_j are given in Appendix D. A few limiting cases follow.

Metallic blob limit

A simple illustrative example is obtained by considering the somewhat extreme case of a high-density "metallic" blob which satisfies $\xi_b >> 1$, while retaining the realistic ordering in the background plasma that the FW wavelength is much longer than the blob radius $\xi << 1$. As the blob density is raised relative to the background, $k_{\perp b}/ k_{\perp}$ becomes a large parameter. Taking this parameter asymptotically large results in M_3 becoming large relative to the other terms. As a result $E_3/E_0 \to 0$ (i.e. the fields vanish within a good conductor) and E_1 is approximated by

$$\frac{E_1}{E_0} = -\frac{W_{0\theta}}{W_{1\theta}} \tag{25}$$

Then taking the subsidiary limit $\xi << 1$, after some algebra employing the small argument expansions of $W_{j\theta}$, we obtain leading order contributions from m = 0, ±1 with the result

$$\frac{E_1}{E_0} = \frac{-i\pi\xi^2}{4}\left[\delta_{m,0} + \left(\frac{Q_i - 1}{Q_i + 1}\right)\delta_{m,1} + \left(\frac{Q_i + 1}{Q_i - 1}\right)\delta_{m,-1}\right] \tag{26}$$

where the purely real quantity $Q_i \equiv -iQ$ and Q was defined after Eq. (7). Larger |m| gives higher order terms in ξ (e.g. m = 2 yields $E_1 \sim \xi^4$) which may therefore be dropped.

For the scattered power, we need the asymptotic form of E_θ for the scattered wave (j = 1) which is

$$E_\theta \sim i\sqrt{\frac{2}{\pi k_\perp r}}e^{i(k_\perp r - \pi/4)}\sum_m e^{im\theta - im\pi/2}E_1 \tag{27}$$

From the expansion of the incident plane wave given in Appendix B, $E_0 = i^{m-1}$ where the incident wave $|E_y|^2$ is normalized to unity. Thus

$$E_\theta \sim -i\xi^2 e^{i(k_\perp r - \pi/4)}\sqrt{\frac{\pi}{8k_\perp r}}\left[1 + e^{i\theta}\left(\frac{Q_i - 1}{Q_i + 1}\right) + e^{-i\theta}\left(\frac{Q_i + 1}{Q_i - 1}\right)\right] \tag{28}$$

Using Eqs. (15) – (17), the effective scattering width is then obtained as

$$\sigma = \frac{\pi^2}{4}k_\perp^3 a_b^4\left[1 + \left(\frac{Q_i - 1}{Q_i + 1}\right)^2 + \left(\frac{Q_i + 1}{Q_i - 1}\right)^2\right] \tag{29}$$

The scattered power fraction is

$$F_P = \frac{\sigma f_p L_x}{\pi a^2} \sim \pi f_p k^3 a^2 L_x \tag{30}$$

so even in the extreme case $f_p \sim 1$ and $kL_x \sim 1$, the scattered power is small in the parameter $\xi^2 = k^2 a_b^2$. We conclude that the metallic blob does not scatter the FW significantly.

Normal blob limit

Next, we consider the more realistic ordering $\xi \sim \xi_b << 1$. Expanding in both ξ and ξ_b results in the leading order terms

$$\frac{E_1}{E_0} = -\frac{i\pi\xi^2}{4}\frac{(Q_{bi}-1)\xi^2-(Q_i-1)\xi_b^2}{(Q_{bi}-1)\xi^2-(Q_i+1)\xi_b^2}\delta_{m,1} - \frac{i\pi\xi^2}{4}\frac{(Q_{bi}+1)\xi^2-(Q_i+1)\xi_b^2}{(Q_{bi}+1)\xi^2-(Q_i-1)\xi_b^2}\delta_{m,-1} \tag{31}$$

$$\frac{E_3}{E_0} = \frac{\xi}{\xi_b}\delta_{m,0} + \frac{2\xi^2}{(Q_i+1)\xi_b^2-(Q_{bi}-1)\xi^2}\delta_{m,1} + \frac{2\xi^2}{(Q_{bi}+1)\xi^2-(Q_i-1)\xi_b^2}\delta_{m,-1} \tag{32}$$

As a check, we see that $E_1 = 0$ and $E_3 = 1$ for $\xi = \xi_b$ and $Q = Q_b$ (i.e. "blob" indistinguishable from background). In order of magnitude, we have

$$\frac{E_1}{E_0} \sim O(\xi^2)\delta_{m,1} + O(\xi^2)\delta_{m,-1} \tag{33}$$

$$\frac{E_3}{E_0} = O(1)\delta_{m,0} + O(1)\delta_{m,1} + O(1)\delta_{m,-1} \tag{34}$$

so that $E_1/E_0 \sim O(\xi^2)$ still holds, just as in the metallic blob limit. As a result the scattering width is also small in the present case.

Scattering-induced mode conversion

When $k_s >> k_f$, where subscripts s and f refer to the SW and FW respectively, the SW amplitudes may be determined perturbatively from

$$E_2 D_2 - E_4 D_4 = -E_0 D_0 - E_1 D_1 + E_3 D_3 \tag{35}$$

$$E_2 W_{2z} - E_4 W_{4z} = 0 \tag{36}$$

where use has been made of the fact that E_z for the FW is negligible. Solving these equations yields

$$E_2 = \frac{S_f W_{4z}}{W_{4z} D_2 - D_4 W_{2z}} \tag{37}$$

$$E_4 = \frac{S_f W_{2z}}{W_{4z} D_2 - D_4 W_{2z}} \tag{38}$$

where the FW driving source term is

$$S_f = -E_0 D_0 - E_1 D_1 + E_3 D_3 \tag{39}$$

When the denominator vanishes, i.e. when

$$W_{4z} D_2 = D_4 W_{2z} \tag{40}$$

we have a slow wave scattering resonance (SWSR). The perturbation theory clearly breaks down at such points, but they are nonetheless expected to define points of enhanced scattering and FW $\rightarrow$ SW conversion. Using the result in Appendix D, the SWSR occurs when

$$\frac{\varepsilon_{\perp} k_{\perp s} L H'_{ms} + \varepsilon_{\times} \dfrac{m}{a_b} L H_{ms}}{H_{ms}} = \frac{\varepsilon_{\perp b} k_{\perp bs} L_b J'_{mbs} + \varepsilon_{\times b} \dfrac{m}{a_b} L_b J_{mbs}}{J_{mbs}} \tag{41}$$

Here $H_{ms} = (H_m)_s \equiv H_m(k_{\perp s} a_b)$ indicates that the Bessel function is evaluated at the slow wave root of the dispersion relation. L is defined in Eq. (B13).

To gain some insight into the possibility of SWSR, consider the case m = 0:

$$\frac{\varepsilon_{\perp}}{\varepsilon_{\perp} - n_{\parallel}^2} \frac{\xi_s H'_{0s}}{H_{0s}} = \frac{\varepsilon_{\perp b}}{\varepsilon_{\perp b} - n_{\parallel}^2} \frac{\xi_{bs} J'_{0bs}}{J_{0bs}} \tag{42}$$

For real arguments of all the Bessel functions (i.e. a propagating SW both in the blob and background) the LHS is complex while the RHS is pure real, thus no resonance is possible. However, if we consider the case of an evanescent SW in the background plasma (ξ_s pure imaginary and positive) then $\xi_s H'_{0s} / H_{0s}$ is real while for ξ_{bs} either real and positive or pure imaginary and positive $\xi_{bs} J'_{0bs} / J_{0bs}$ is real. In these cases, a solution is possible. In particular for the case of ξ_{bs} real, the RHS is qualitatively tan-like covering the range $(-\infty, \infty)$ and will admit solutions when the argument ξ_{bs} is of order unity or larger. Such a solution corresponds to a SW-blob "bound state". Normally, SW propagation in the blob, but evanescence in the background will require that the "blob" have lower density than the background, and is thus not a blob but a "hole". Thus we conclude that SWSR can occur when a hole is large enough to admit one or more SW wavelengths. In practice isolated holes are not likely to occur in the SOL, but the implication is that there could be FW $\rightarrow$ SW conversion at the turbulent edge of the plasma when the turbulence scale size is comparable to the SW wavelength.

In the absence of a SWSR, the validity condition for the perturbation expansion can be determined by demanding a typical SW term in the E_θ equation be small compared with a typical FW term, e.g. $E_2 W_{2\theta} << E_3 W_{3\theta}$. This estimate can be shown to require $|\xi_s| >>1$. Intuitively we expect the SW coupling to be negligible in the FW equations when $k_f << k_s$ which is usually satisfied when $\varepsilon_{||} >> \varepsilon_\perp$. However, here the FW wavelength is forced to be $k_f \sim m/a_b$ near the blob, so for $m \sim 1$ the decoupling condition $k_f << k_s$ reduces to $|\xi_s| >>1$.

IV. Scattering of an incident slow wave

SW limit of the formalism

For this application, the index p in Eq. (8) corresponds to the SW. In the interest of simplicity, the calculation will be restricted to the electrostatic limit. In this case L in Eq. (B13) reduces to $L = i/k_z$ and since $\Phi = LE_z$, matching of Φ on the surface of the blob matches both E_θ and E_z. Consequently, the two relevant matching conditions from the set Eqs. (9) – (12) are for D and W_z (i.e. W_θ is redundant). Neglecting the coupling to the FW, we obtain the 2×2 system of equations

$$E_1 D_1 - E_3 D_3 = -E_0 D_0 \tag{43}$$

$$E_1 W_{1z} - E_3 W_{3z} = -E_0 W_{0z} \tag{44}$$

with coefficients given in Appendix D. The solution is

$$\frac{E_1}{E_0} = \frac{W_{3z}D_0 - W_{0z}D_3}{W_{1z}D_3 - W_{3z}D_1} \tag{45}$$

$$\frac{E_3}{E_0} = \frac{W_{1z}D_0 - W_{0z}D_1}{W_{1z}D_3 - W_{3z}D_1} \tag{46}$$

Typical parameters for LH waves in the SOL suggest that plasma effects enter mainly through $\varepsilon_{||}$, i.e. $\varepsilon_\perp \approx 1$ and $\varepsilon_\times << 1$ which is the limit considered in the following. In this case, the scattered slow wave is given by

$$\frac{E_1}{E_0} = \frac{J_{mb}\xi J'_m - J_m \xi_b J'_{mb}}{H_m \xi_b J'_{mb} - J_{mb}\xi H'_m} \equiv S_m(\xi, \xi_b) \tag{47}$$

Note that For $\xi = \xi_b$, E_1 vanishes as it should. For clarity in the next steps, we revert to a more explicit notation

$$E_m^{(1)} = E_0 S_m(\xi, \xi_b) = i^m S_m(\xi, \xi_b) \tag{48}$$

and here the incident wave is normalized with $E_z = 1$.

The S_m, which gives the waves at the blob interface, are related to the scattering coefficients A_m using the Bessel coefficients for the SW, and their asymptotic forms, as given in Appendix D. The asymptotic form of E_z for the scattered wave is

$$E_z^{(1)} = \sum_m e^{im\theta} i^m S_m(\xi, \xi_b) H_m(k_\perp r) \rightarrow \sum_m e^{im\theta} S_m \sqrt{\frac{2}{\pi k_\perp r}} e^{i(k_\perp r - \pi/4)} \tag{49}$$

The effective scattering width is then obtained as

$$\frac{\sigma}{a_b} = \frac{2\pi r}{a_b} \frac{2}{\pi k_\perp r} \sum_m |S_m|^2 = \frac{4}{\xi} \sum_m |S_m(\xi, \xi_b)|^2 \tag{50}$$

It is also useful to define the differential scattering width

$$\frac{\sigma(\theta)}{a_b} = \frac{2}{\pi\xi} \left| \sum_m S_m(\xi, \xi_b) e^{im\theta} \right|^2 \tag{51}$$

with $\int d\theta\, \sigma(\theta) = \sigma$. A good diagnostic of the angular distribution of the scattered power (as $r \rightarrow \infty$) is therefore the normalized differential scattering width

$$\hat{\sigma}(\theta) = \frac{\sigma(\theta)}{\sigma} = \frac{\left|\sum_m S_m(\xi,\xi_b) e^{im\theta}\right|^2}{2\pi \sum_m \left|S_m(\xi,\xi_b)\right|^2} \tag{52}$$

which on average is $1/2\pi$.

From the general result of Eq. (47), together with Eq. (50), it is seen that that $\sigma \sim a_b$ for $\xi \sim \xi_b \sim 1$. The ratio of scattered to incident power F_P in Eq. (18) or (20) will be of order unity when one or more blobs ($N_b \geq 1$) is encountered is a poloidal swath of plasma of width $L_y \sim \sigma \sim a_b$ as the rf traverses the SOL.

In the next sub-sections various regimes of Eq. (47) ($\xi_b \to \infty$, $\xi << 1$, $\xi \sim 1$ and, $\xi >> 1$) are considered by analytical expansion and by direct numerical evaluation of the general result. For completeness it should be noted here that in the tenuous plasma regime the SW is a backward propagating mode. However, as discussed in Appendix E, this fact is inconsequential for the scattering solutions.

Metallic blob limit

As in the FW case, some useful insights are gained by first considering the metallic blob (i.e. metal cylinder) limit in which $\xi_b \to \infty$. From Eq. (46) using the results of Appendix D it follows that $E_3 = 0$ in this limit, as expected. Then from Eq. (47)

$$\frac{E_1}{E_0} = S_m = -\frac{J_m}{H_m} \tag{53}$$

In the $\xi << 1$ sublimit the dominant contribution comes from m = 0

$$S_0 = \frac{i\pi}{2\gamma_E - i\pi + 2\ln(\xi/2)} \tag{54}$$

where $\gamma_E = 0.577\ldots$ is Euler's constant. The scattering width follows as

$$\sigma = \frac{4}{k_\perp} \sum_m \left|S_0\right|^2 = \frac{4}{k_\perp} \frac{1}{[2\gamma_E/\pi + (2/\pi)\ln(\xi/2)]^2 + 1} \tag{55}$$

It is also straightforward to treat the insulating blob limit ($\xi_b = 0$) analytically. Note the scaling $\sigma \sim 1/k_\perp$ in this long-wavelength metallic blob limit, *independent of the blob size.*

LH scattering: long wavelength limit

In general, the (far-field) long-wavelength regime is obtained when $\xi << 1$ without demanding large ξ_b. As an example, the scattering width for $\xi = 0.1$ and varying values of ξ_b is shown in Fig. 2. Note that a typical value of σ is of order $1/k_\perp$ not a_b (i.e. $\sigma/a_b \sim 1/\xi \sim 10$ here). This means that the blob causes long range perturbations, on the order of the wavelength which is much greater than the blob size, when $\xi << 1$. Even larger values of σ occur near scattering resonances, where the denominator of S_m is small. The broad feature near $\xi_b = 1$ is related to a weak m = 0 resonance, and the sharp spike near $\xi_b = 2.4$ is a strong m = 1 resonance. Scattering resonances are studied further in the next sub-section. Except near the scattering resonances, the results for $\xi_b > 1$ are of the order-of-magnitude predicted by the metallic blob limit with $\xi << 1$.

The field pattern for $\xi_b = 0.9$ is shown in Fig. 3. The differential scattering width (not shown) is essentially independent of θ, but interference of the scattered and incident waves occurs, giving rise to the observed pattern.

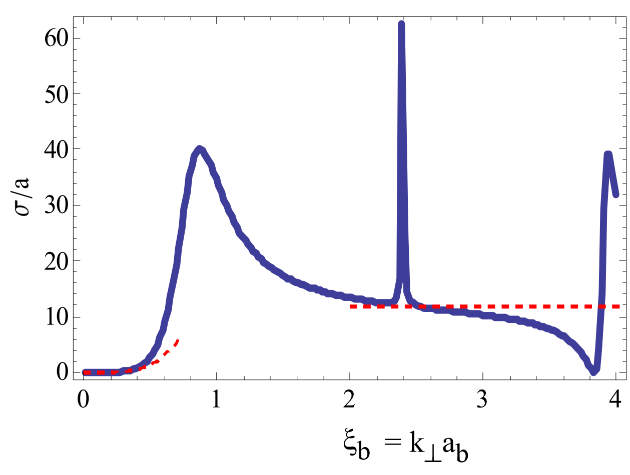

Fig. 2 (color online) Scattering width normalized to the blob size a_b for the case $\xi = 0.1$. Asymptotic results for ξ, $\xi_b << 1$ and for the metallic blob limit with $\xi << 1$ are shown in dashed red. Note the strong scattering resonance at $\xi_b = 2.4$.

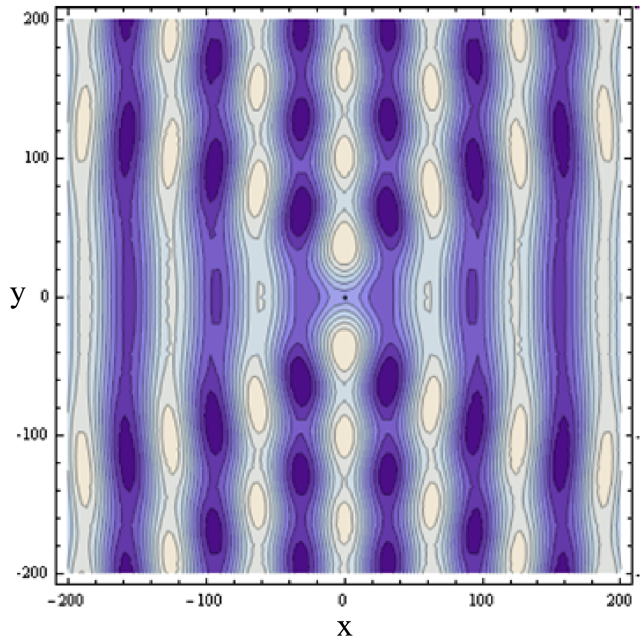

Fig. 3 (color online) Field pattern Re(E_z) for the same case as Fig 2 at ξ_b = 0.9. The incident wave is coming from the left. The blob is the tiny (almost invisible) dot at the center of the figure, x = y = 0.

LH-blob scattering resonance

Blob scattering resonances can occur for special values of the parameters. The m = 1 resonance in Fig. 2 is very sharp for two reasons. First, parameters in the blob interior (i.e. ξ_b of order unity) permit a SW wavelength to fit inside the blob. Second, $\xi \ll 1$ implies that the radiation damping of the scattered wave ($\sim k_\perp$) is small, and therefore an approximate "bound state" exists. This particular resonance is an m = 1 resonance, and is shown in more detail in Figs. 4 and 5.

Figure 4 shows the field pattern. The incident wave energy is coming in from the left in all field pattern figures in this paper. The m = 1 character is clearly evident from the inset figure, which shows an enlarged view of the blob itself. The angular distribution of scattered power, i.e. the normalized differential cross-section $\hat{\sigma}(\theta)$ is shown in Fig. 5. Both forward and backward scattering are enhanced relative to the non-resonant case of Fig. 3.

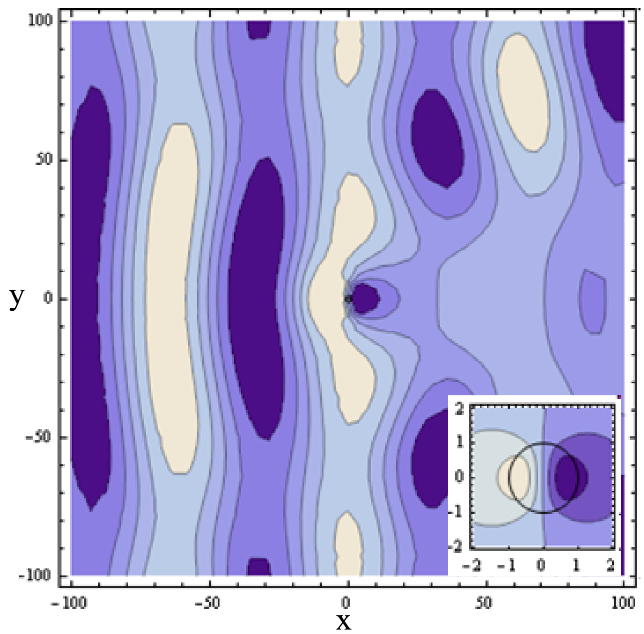

Fig. 4 (color online) Field pattern Re(E_z) for the m = 1 scattering resonance at ξ_b = 2.4, ξ = 0.1 (also see Fig 2). The inset figure shows an enlarged view of the blob region.

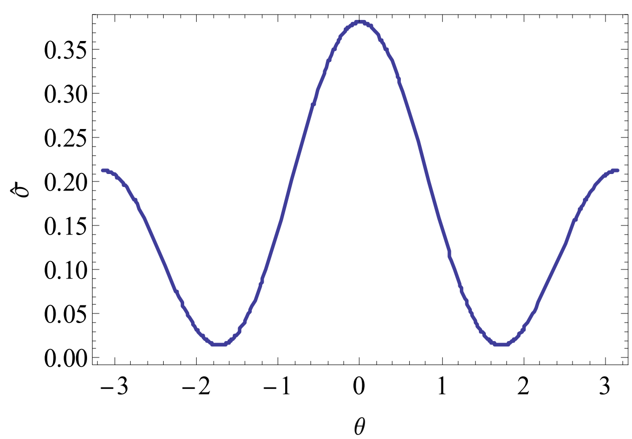

Fig. 5 (color online) Normalized differential scattering cross-section for the same case as Fig. 4. Forward scattering corresponds to θ = 0.

LH scattering: short wavelength limit

Finally, we consider a moderately short wavelength by taking $\xi = 3$ and examine the scattering for disparate ξ_b. First, the case $\xi_b = 0.1$ is shown in Fig. 6. In this case, since $\xi_b < \xi$ the SW dispersion relation typically requires lower density inside the cylinder, i.e. the blob is actually a hole. For comparison, the case $\xi_b = 10$ is shown in Fig. 7. Both cases illustrate the phenomenon of shadowing, which is expected when waves encounter an object much larger than its wavelength. Both back-scattering and small-angle forward scattering are possible in this regime.

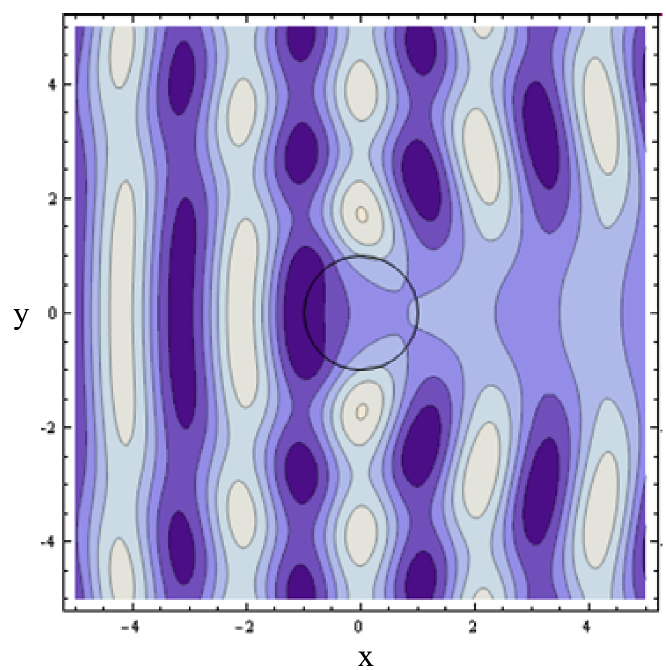

Fig. 6 (color online) Field pattern Re(E_z) for the case $\xi_b = 0.1$, $\xi = 3$. The blob (here actually a hole) is shown by the black circle. Note the shadowed wedge for x > 0.

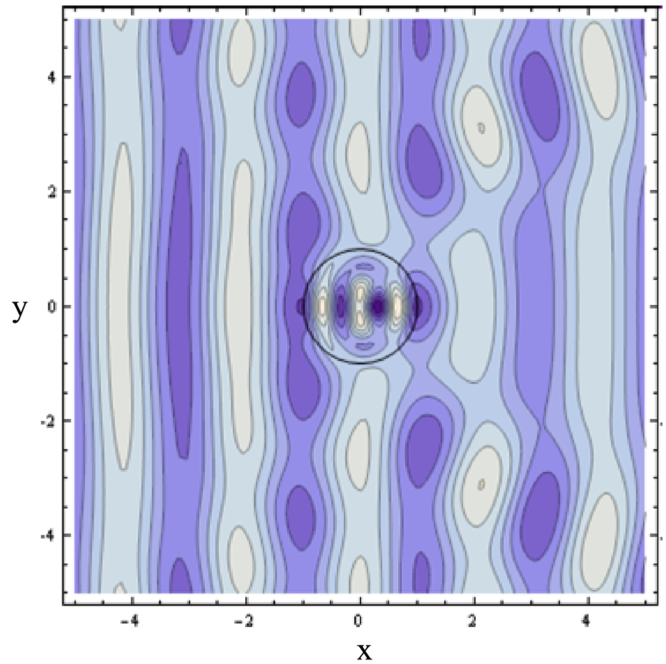

Fig. 7 (color online) Field pattern Re(E_z) for the case ξ_b = 10, ξ = 3. The blob is shown by the black circle.

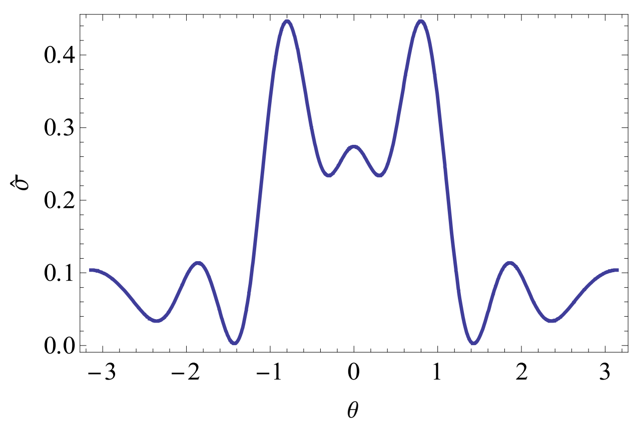

Fig. 8 (color online) Normalized differential scattering width for the same case as Fig. 7. Small-angle forward scattering “ears” are prominent.

V. Conclusions

In this paper we have investigated rf scattering from isolated field-aligned cylindrical blob-filaments. While the formalism presented in Sec. II is for the most part general, applications have focused on two cases: incident ICRF fast waves and incident LH slow waves.

Fast wave scattering is typically, and not surprisingly, found to be small in the ratio of the wavelength $2\pi/k_\perp$ to the blob radius a_b in the plane perpendicular to B. The scattering width is given by Eq. (29) and scales as $\sigma \propto k_\perp^3 a_b^4$ while the fraction of incident power that is scattered is given by Eq. (30). The scattered power is small enough that it is unlikely to be of direct concern as a power loss channel.

However, the FW scattering analysis also showed that scattering-induced mode conversion of FWs to SWs is possible. This process is expected to be strong when the scale length of blobs (or holes) is comparable to the slow-wave wavelength. The present calculation must be regarded as suggestive and qualitative because only the breakdown of the perturbation expansion in the size of the SW relative to the FW was demonstrated in Eqs. (37) and (38). It is important to note that the conversion of even a small fraction of FW power into the SW branch could be significant for edge interactions involving rf-sheaths at the plasma-facing surfaces.

Scattering of an incident slow wave is found to be significant, as expected from previous work that employed a density fluctuation formalism.[6-8] Since the SW wavelength for LH waves can be order-of-magnitude comparable to the size of turbulent blob structures, various regimes of the critical parameter $\xi = k_\perp a_b$ are of interest. A typical value of the scattering width σ is the larger of $1/k_\perp$ and a_b. In particular, for small $\xi << 1$ the blob perturbs the rf fields on a space scale of the order of a wavelength, even though the blob radius is much smaller (Fig. 3). The $\xi << 1$ regime is very different for SWs than for FWs (where scattering is negligible) because of the wave polarization. Other scattering phenomena were also demonstrated, including the existence of slow-wave scattering resonances (Figs. 2 and 4), and for $\xi >> 1$, rf-wave shadowing (Fig. 5) and small-angle forward scattering.

The present calculations only treat the single-blob limit. If the packing fraction of the blobs is sufficiently dense relative to the wavelength, then scattering from several near-by blobs can be correlated and the approach taken here breaks down. While the single blob limit is of interest in the far SOL, the many-blob-hole limit would be expected to apply closer in towards the separatrix. Results here suggest that a numerical investigation of LH blob scattering, and of ICRF blob scattering retaining induced mode conversion, would be interesting. Finally, in addition to rf physics applications such as power loss and edge interaction, rf blob scattering may be of interest as a tool for diagnosing turbulent structures in the edge and SOL plasmas.

Acknowledgments

Discussions with the rf SciDAC team are gratefully acknowledged. This work was supported by the U.S. Department of Energy (DOE) under grants DE-FG02-97ER54392 and DE-FC02-05ER54823; however, such support does not constitute an endorsement by the DOE of the views expressed herein.

Appendix A: Fast and slow wave equations in a cylinder

In this appendix, we obtain reduced wave equations for the FW and SW in cylindrical geometry. The starting point is the wave equation

$$-\lambda_0^2 \nabla \times \nabla \times \mathbf{E} + \varepsilon \cdot \mathbf{E} = 0 \tag{A1}$$

where $\lambda_0 = c/\omega$ and modes vary like $\exp(im\theta + ik_{||}z - i\omega t)$. For the cold-fluid plasma model given by Eq. (1) and taking $\mathbf{B}_0$ along z

$$\varepsilon \cdot \mathbf{E} = \mathbf{e}_r\left[\varepsilon_\perp E_r - i\varepsilon_\times E_\theta\right] + \mathbf{e}_\theta\left[\varepsilon_\perp E_\theta + i\varepsilon_\times E_r\right] + \mathbf{e}_z\left[\varepsilon_{||} E_z\right] \tag{A2}$$

The complete wave equation in cylindrical coordinates therefore has the components

$$-\lambda_0^2\left[k_z^2 E_r + \frac{m^2}{r^2}E_r + \frac{im}{r^2}\frac{d}{dr}(rE_\theta) + ik_z\frac{dE_z}{dr}\right] + \left[\varepsilon_\perp E_r - i\varepsilon_\times E_\theta\right] = 0 \tag{A3}$$

$$-\lambda_0^2\left[\mathrm{im}\frac{d}{dr}\left(\frac{E_r}{r}\right)+k_z^2E_\theta-\frac{d}{dr}\left(\frac{1}{r}\frac{d}{dr}(rE_\theta)\right)-\frac{k_zm}{r}E_z\right]+\left[\varepsilon_\perp E_\theta+i\varepsilon_\times E_r\right]=0 \tag{A4}$$

$$-\lambda_0^2\left[\frac{ik_z}{r}\frac{d}{dr}(rE_r)-\frac{k_zm}{r}E_\theta-\frac{1}{r}\frac{d}{dr}\left(r\frac{dE_z}{dr}\right)+\frac{m^2}{r^2}E_z\right]+\left[\varepsilon_\parallel E_z\right]=0 \tag{A5}$$

FW equations

The FW ordering $\varepsilon_\parallel >> \varepsilon_\perp \sim n_\perp^2 \sim n_\parallel^2$ implies that $\varepsilon_\parallel$ is the largest parameter in the problem, therefore Eq. (A5) renders E_z negligible in lowest order. The remaining equations can be manipulated to obtain

$$\left(\varepsilon_\perp-n_\parallel^2-\lambda_0^2\frac{m^2}{r^2}\right)E_r=i\varepsilon_\times E_\theta+\lambda_0^2\frac{\mathrm{im}}{r^2}\frac{d}{dr}(rE_\theta) \tag{A6}$$

$$\lambda_0^2\frac{d}{dr}\left(\frac{1}{r}\frac{d}{dr}(rE_\theta)\right)+(\varepsilon_\perp-n_\parallel^2)E_\theta+i\varepsilon_\times E_r-\mathrm{im}\lambda_0^2\frac{d}{dr}\left(\frac{E_r}{r}\right)=0 \tag{A7}$$

SW equations

The SW ordering is $\varepsilon_\parallel \sim n_\perp^2 >> \varepsilon_\perp \sim n_\parallel^2$. Since we anticipate cancellations, small terms are retained on the right-hand-side (RHS) of the equations to yield the (still exact) forms

$$-\lambda_0^2\frac{m^2}{r^2}E_r-\lambda_0^2\frac{\mathrm{im}}{r^2}\frac{d}{dr}(rE_\theta)=\lambda_0^2ik_z\frac{dE_z}{dr}-(\varepsilon_\perp-n_\parallel^2)E_r+i\varepsilon_\times E_\theta \tag{A8}$$

$$-\lambda_0^2\mathrm{im}\frac{d}{dr}\left(\frac{E_r}{r}\right)+\lambda_0^2\frac{d}{dr}\left(\frac{1}{r}\frac{d}{dr}(rE_\theta)\right)=-\lambda_0^2\frac{k_zm}{r}E_z-(\varepsilon_\perp-n_\parallel^2)E_\theta-i\varepsilon_\times E_r \tag{A9}$$

$$\lambda_0^2\frac{1}{r}\frac{d}{dr}\left(r\frac{dE_z}{dr}\right)-\lambda_0^2\frac{m^2}{r^2}E_z+\varepsilon_\parallel E_z=\lambda_0^2\frac{ik_z}{r}\frac{d}{dr}(rE_r)-\lambda_0^2\frac{k_zm}{r}E_\theta \tag{A10}$$

Next, assuming that $\varepsilon_\perp$ and $\varepsilon_\parallel$ are constants, Eqs. (A8) and (A9) may be manipulated to get equations for $(\varepsilon_\perp-n_\parallel^2)\nabla_\perp\cdot\mathbf{E}$ and $(\varepsilon_\perp-n_\parallel^2)\mathbf{e}_z\cdot\nabla\times\mathbf{E}$.

$$0 = i\lambda_0^2 k_z \nabla_\perp^2 E_z - (\varepsilon_\perp - n_\parallel^2)\nabla_\perp \cdot \mathbf{E} + i\varepsilon_\times \mathbf{e}_z \cdot \nabla \times \mathbf{E} \tag{A11}$$

$$-\lambda_0^2 \nabla_\perp^2 (\mathbf{e}_z \cdot \nabla \times \mathbf{E}) = (\varepsilon_\perp - n_\parallel^2)\mathbf{e}_z \cdot \nabla \times \mathbf{E} + i\varepsilon_\times \nabla_\perp \cdot \mathbf{E} \tag{A12}$$

Note that in Eq. (A11) the LHS has cancelled out, while in Eq. (A12) it remains. Thus in the SW ordering $\mathbf{e}_z \cdot \nabla \times \mathbf{E} / \nabla \cdot \mathbf{E}$ is small in $n_\perp^2 / \varepsilon_\perp << 1$. This justifies the quasi-electrostatic approximation for the *perpendicular* electric fields, viz.

$$\mathbf{E}_\perp = -\nabla_\perp \Phi \tag{A13}$$

Then the two coupled equations describing the SW come from Eqs. (A10) and (A11) and are

$$(\varepsilon_\perp - n_\parallel^2)\nabla_\perp^2 \Phi + ik_z \lambda_0^2 \nabla_\perp^2 E_z = 0 \tag{A14}$$

$$ik_z \lambda_0^2 \nabla_\perp^2 \Phi + \lambda_0^2 \nabla_\perp^2 E_z + \varepsilon_\parallel E_z = 0 \tag{A15}$$

Appendix B: Solution of the wave equations

The expansion of the incoming plane wave in cylindrical coordinates is central to the scattering problem. For a scalar field, the required identity is just

$$e^{i\xi \cos\theta} = \sum_{m=-\infty}^{\infty} i^m J_m(\xi) e^{im\theta} \tag{B1}$$

where for the plane wave $\xi = k_\perp r$. Here, we need to perform the plane wave expansion in cylindrical coordinates for the vector electric fields with polarizations corresponding to the fast and slow waves. From this, a general solution of the wave equations will become apparent.

FW equations

Consider an incoming plane FW with $k_y = 0$. In Cartesian coordinates, the FW electric field vector has the polarization

$$\mathbf{E} = (\mathbf{e}_y + Q\mathbf{e}_x)\, e^{ik_\perp x} \tag{B2}$$

where

$$Q = \frac{i\varepsilon_\times}{\varepsilon_\perp - n_\parallel^2} \tag{B3}$$

and $k_\perp$ satisfies the FW dispersion relation

$$n_\perp^2 = \frac{(\varepsilon_\perp - n_\parallel^2)^2 - \varepsilon_\times^2}{\varepsilon_\perp - n_\parallel^2} \tag{B4}$$

From this solution, we transform from Cartesian to cylindrical coordinates directly, using $x = r\cos\theta$, $y = r\sin\theta$, $\mathbf{e}_x = \mathbf{e}_r \cos\theta - \mathbf{e}_\theta \sin\theta$, $\mathbf{e}_y = \mathbf{e}_r \sin\theta + \mathbf{e}_\theta \cos\theta$. The result is

$$\mathbf{E} = \left(\mathbf{e}_r Q\cos\theta - \mathbf{e}_\theta Q\sin\theta + \mathbf{e}_r \sin\theta + \mathbf{e}_\theta \cos\theta\right) e^{ik_\perp r\cos\theta} \tag{B5}$$

which is converted by Bessel identities to

$$E_\theta = \sum_m i^{m-1}\left(J_m' + \frac{imQJ_m}{k_\perp r}\right) e^{im\theta} \tag{B6}$$

$$E_r = \sum_m i^{m-1}\left(\frac{-imJ_m}{k_\perp r} + QJ_m'\right) e^{im\theta} \tag{B7}$$

where $J_m = J_m(k_\perp r)$.

In Appendix A the FW equation in cylindrical coordinates was derived. The coupled equations for E_θ and E_r are separable in r and θ. It follows that each individual term in the above plane wave expansion must be a solution of the wave equations. It can be shown that this is the case when $k_\perp$ satisfies the FW dispersion relation. Thus the general solution of the wave equation can be constructed as

$$E_\theta = \sum_m E_m W_{\theta m}(r)\, e^{im\theta} \tag{B8}$$

$$E_r = \sum_m E_m W_{rm}(r) e^{im\theta} \tag{B9}$$

where the E_m are arbitrary constants, and for regular BCs at r = 0

$$W_{\theta m} = J'_m + \frac{imQJ_m}{k_\perp r} \tag{B10}$$

$$W_{rm} = \frac{-imJ_m}{k_\perp r} + QJ'_m \tag{B11}$$

In general, a linear combination of J_m and Y_m are permitted; e.g. for outgoing wave boundary conditions $J_m \rightarrow H_m^{(1)}$ where $H_m^{(1)}$ is the outgoing Hankel function.

SW equations

Next, consider an incoming plane SW with $k_y = 0$. In Cartesian coordinates, the field components of the SW are related by [see Eq. (A14)]

$$\Phi = LE_z \tag{B12}$$

$$L = \frac{-ik_z\lambda_0^2}{\varepsilon_\perp - n_\parallel^2} \tag{B13}$$

The electric field polarization for the SW is of the form

$$\mathbf{E} = (\mathbf{e}_z - i\mathbf{k}_\perp L) e^{ik_\perp x} \tag{B14}$$

where $k_\perp$ satisfies the SW dispersion relation

$$n_\perp^2 \varepsilon_\perp + n_\parallel^2 \varepsilon_\parallel = \varepsilon_\perp \varepsilon_\parallel \tag{B15}$$

Following the same logic as for the FW, the general SW solution takes the form

$$E_r = -\sum_m E_m k_\perp L J'_m e^{im\theta} \tag{B16}$$

$$E_\theta = -\sum_m E_m \frac{im}{r} L J_m e^{im\theta} \tag{B17}$$

$$E_z = \sum_m E_m J_m e^{im\theta} \tag{B18}$$

where again, depending on BCs, a linear combination of J_m and Y_m are permitted wherever J_m appears. It may be verified directly that Eqs. (B16) – (B18) indeed satisfy the SW wave equation for constant $\varepsilon_\perp$ and $\varepsilon_\parallel$.

Appendix C: Poynting flux and scattered power

The Poynting flux is

$$\mathbf{S} = \frac{c}{16\pi}\mathbf{E}\times\mathbf{B}^* + cc \tag{C1}$$

Given the wave polarization of the scattered waves, one can calculate the asymptotic power in each m component and ratio of scattered power per blob to the total incident power.

Fast waves

Neglecting E_z and taking x as a radial variable (in a local coordinate system asymptotically far from the source) $S_x = (c/16\pi)E_y B_z^* + cc$, therefore using $B_z = n_x E_y$

$$S_r = \frac{k_r c^2}{8\pi\omega}|E_\theta|^2 \tag{C2}$$

which applies to both incoming (k_x, E_y) and scattered (k_r, E_θ) waves. Since the plasma dispersion is the same, incoming and scattered waves also have the same $k_\perp = k_x = k_r$. The incoming incident power is

$$P_{inc} = \int dA\, S_x = \frac{k_x c^2 L_y L_z}{8\pi\omega}|E_y|^2 \tag{C3}$$

where L_y and L_z are the dimension of the incoming rf beam. The scattered power is

$$P_{sca} = \int dA\, S_r = \int d\theta\, r L_z \frac{k_r c^2}{8\pi\omega}|E_\theta|^2 \tag{C4}$$

and the ratio of scattered (subscript 1) to incident (subscript 0) power is

$$\frac{P_{sca}}{P_{inc}} = \frac{r}{L_y}\int d\theta \frac{|E_{\theta 1}|^2}{|E_{y0}|^2} \tag{C5}$$

For the FW it is convenient to express the scattering amplitudes in the form

$$\left.\frac{E_{\theta 1}}{E_{y0}}\right|_{r\to\infty} = \sum_m A_m e^{im\theta} \tag{C6}$$

Then

$$\frac{P_{sca}}{P_{inc}} = \frac{2\pi r}{L_y}\sum_m |A_m|^2 \tag{C7}$$

Slow waves

For the slow wave polarization, neglecting B_z, the Poynting flux is given by $S_x = -(c/16\pi)E_z B_y^* + cc$ and using $B_y = -n_x(1+ik_{\|}L)E_z$ where L is defined in Eq. (B13) we find the Poynting flux for the incident wave is

$$S_x = -\frac{c}{8\pi}\frac{n_x \varepsilon_\perp}{n_{\|}^2 - \varepsilon_\perp}|E_z|^2 \tag{C8}$$

and for the scattered wave, it is

$$S_r = -\frac{c}{8\pi}\frac{n_r \varepsilon_\perp}{n_{\|}^2 - \varepsilon_\perp}|E_z|^2 \tag{C9}$$

In the quasi-electrostatic limit employed in the main text, one can further invoke $n_{\|}^2 >> \varepsilon_\perp$ to simplify these expressions.

Analogous to the FW case, the ratio of scattered (subscript 1) to incident (subscript 0) power is

$$\frac{P_{sca}}{P_{inc}} = \frac{r}{L_y}\int d\theta \frac{|E_{z1}|^2}{|E_{z0}|^2} \tag{C10}$$

For the SW it is convenient to express the scattering amplitudes in the form

$$\left.\frac{E_{z1}}{E_{z0}}\right|_{r\to\infty} = \sum_m A_m e^{im\theta} \tag{C11}$$

Then, Eq. (C7) gives the ratio of scattered to incident SW power.

Note that the SW can be a backward propagating mode, i.e. for positive (right-going) Poynting flux and group velocity $\partial\omega/\partial k_x$, the phase velocity ω/k_x is negative.

Appendix D: Bessel scattering coefficients

In this appendix, we give the vector components of the FW and SW solutions to the respective wave equations in cylindrical geometry, Eqs. (2) − (5), adopting the notation of Eq. (6). These coefficients are obtained from Eqs. (B10), (B11), (B16), (B17) and (B18).

In the following $\xi = k_\perp r$ and for the matching conditions $\xi = k_\perp a_b$. All Bessel functions are evaluated at ξ (or $\xi_b = k_{\perp b} r$ where $k_{\perp b}$ is from the dispersion relation using blob plasma parameters). H_m is the outgoing Hankel function.

Incident fast waves

Considering an incident FW, but allowing for both types of scattered wave, the subscript s denotes the SW root, unadorned k denotes the FW root for $k_\perp$ and the index j = (0, 4) is as described in Eq. (8) with p = f and p′ = s.

$$W_{0\theta} = J'_m + \frac{imQJ_m}{k_\perp r} \tag{D1}$$

$$W_{2\theta} = -\frac{im}{r} L H_{ms} \tag{D2}$$

$W_{1\theta}$ is obtained from $W_{0\theta}$ by the replacement $J_m \to H_m$. $W_{3\theta}$ is obtained from $W_{0\theta}$ by evaluation inside the blob (i.e. $k_\perp \to k_{\perp b}$, $J_m \to J_{mb}$, $Q \to Q_b$ etc.). $W_{4\theta}$ is obtained from $W_{2\theta}$ by first replacing $H_m \to J_m$ and then by invoking evaluation inside the blob.

$$W_{0r} = \frac{-imJ_m}{k_\perp r} + QJ'_m \tag{D3}$$

$$W_{2r} = -k_{\perp s} LH'_{ms} \tag{D4}$$

The rules for obtaining W_{1r}, W_{3r} and W_{4r} are as stated after Eq. (D2). For the z-components, neglecting E_z of the FW

$$W_{2z} = H_{ms} \tag{D5}$$

$$W_{4z} = J_{mbs} \tag{D6}$$

and all other W_{jz} are zero. Here subscript "s" denotes that the Bessel function is to be evaluated at the SW root for $k_\perp$, i.e. $H_{ms} = H_m(k_{\perp s} r)$.

From these elementary quantities we can work out M_j and D_j. For M_0, M_1 and M_3 which are FW quantities, we use Eq. (13) and the Bessel relation

$$\nabla_\perp^2 J_m = -k_\perp^2 J_m \tag{D7}$$

and similarly for H_m.

$$M_0 = -k_\perp J_m \tag{D8}$$

$$M_2 = 0 \tag{D9}$$

M_1, M_3 and M_4 are obtained by the rules stated after Eq. (D2). $M_2 = M_4 = 0$ ($\propto B_z$) has the interpretation that the SW is electrostatic in the x-y plane, having an electromagnetic component only in $E_{||}$ (from $A_{||}$ which does not generate a B_z). Finally

$$D_0 = \varepsilon_\perp W_{0r} - i\varepsilon_\times W_{0\theta} \tag{D10}$$

$$D_2 = -\varepsilon_\perp k_{\perp s} LH'_{ms} - \varepsilon_\times \frac{m}{r} LH_{ms} \tag{D11}$$

with D_1,D_3 and D_4 obtained by the substitution rules.

Incident slow waves

Bessel coefficients are given here for the case of incident and scattered SWs. SW to FW conversion coefficients are not given here, so an unadorned k denotes the SW root for $k_\perp$ and the index j = 0, 1, 3 is as described in Eq. (8) with p = s.

$$W_{0r} = -k_\perp L J'_m \tag{D12}$$

$$W_{0\theta} = -\frac{im}{r} L J_m \tag{D13}$$

$$W_{0z} = J_m \tag{D14}$$

For $\alpha =$ r, θ, z: $W_{1\alpha}$ is obtained from $W_{0\alpha}$ by the replacement $J_m \to H_m$; $W_{3\alpha}$ is obtained from $W_{0\alpha}$ by evaluation inside the blob.

The SW scattering problem also requires the $D_{j\alpha}$ coefficients. In general these have a complicated form, as in Eq. (D10) and (D11). In the tenuous plasma limit, invoked in the main text, and valid for typical LH parameters in the SOL, we have $\varepsilon_\perp \approx 1$, $\varepsilon_\times << 1$ and

$$D_0 = -\frac{ik_\perp}{k_z} J'_m \tag{D15}$$

where we have also invoked the electrostatic limit for $L \approx i/k_z$. $D_{1\alpha}$ is obtained from $D_{0\alpha}$ by the replacement $J_m \to H_m$; $D_{3\alpha}$ is obtained from $D_{0\alpha}$ by evaluation inside the blob.

Appendix E: Backward propagation and the slow wave

In some regimes, notably the tenuous plasma regime discussed in the main text, the SW is a backward propagating mode, i.e. the phase and group velocities are in opposite directions. In this case, the incident wave that carries energy in the positive x direction has $k_x < 0$. This can be taken into account in the formalism in several ways. The most straightforward is to rewrite all results using $k_\perp = -k_x$ and an incident wave of the form $\exp(-ik_\perp x) = \exp(-i\xi \cos\theta)$. If this is done, one finds that $J_m \to J_{-m}$, $H_m \to$

H_{-m} everywhere, and for an outgoing wave, the appropriate Hankel function is now $H_{-m}^{(2)}$ instead of $H_{-m}^{(1)}$. However, owing to Bessel function symmetries, neither the scattered field patterns ~ Re(**E**) nor the scattering widths are modified.

Physically this invariance is because the scattering problem does not follow the waves in time (we can examine the solutions at the time $-i\omega t = 0$) so the effect of positive or negative k_x enters as a complex conjugation operation which does not affect the physical field ~ Re(**E**).

References

[1] S. J. Zweben, J. A. Boedo, O. Grulke, C. Hidalgo, B. LaBombard, R. J. Maqueda, P. Scarin and J. L. Terry, Plasma Phys. Control. Fusion **49**, S1 (2007); and earlier review papers referenced therein.

[2] S. I. Krasheninnikov, D. A. D'Ippolito, and J. R. Myra, J. Plasma Physics **74**, 679 (2008).

[3] D.A. D'Ippolito, J. R. Myra, S.I. Krasheninnikov, G.Q. Yu and A. Yu. Pigarov, Contrib. Plasma Phys. **44**, 205 (2004).

[4] V. Pericoli-Ridolfini, L. Giannone, and R. Bartiromo, Nucl. Fusion **34**, 469 (1994).

[5] J. D. Moody, M. Porkolab, C. L. Fiore, F. S. McDermott, Y. Takase, J. Terry, and S. M. Wolfe, Phys. Rev. Lett. **60**, 298 (1988).

[6] P. T. Bonoli and E. Ott, Phys. Rev. Lett. **46**, 424 (1981).

[7] P. L. Andrews and F. W. Perkins, Phys. Fluids **26**, 2537 (1983).

[8] K. Hizanidis, A. K. Ram, Y. Kominis, and C. Tsironis, Phys. Plasmas **17**, 022505 (2010).

[9] P. M. Morse and H. Feshbach, in *Methods of Theoretical Physics*, (McGraw-Hill, New York, 1953), Part II, pp. 1376 – 1382.